iJRASET
International Journal For Research in Applied Science and Engineering Technology

INTERNATIONAL JOURNAL FOR RESEARCH

IN APPLIED SCIENCE & ENGINEERING TECHNOLOGY

Volume: 12 **Issue:** VIII **Month of publication:** August 2024

DOI: https://doi.org/10.22214/ijraset.2024.63874

www.ijraset.com

Call: 08813907089 | E-mail ID: ijraset@gmail.com

International Journal for Research in Applied Science & Engineering Technology (IJRASET)
ISSN: 2321-9653; IC Value: 45.98; SJ Impact Factor: 7.538
Volume 12 Issue VIII Aug 2024- Available at www.ijraset.com

Natural Synthesis, Characterization, and Photocatalytic Performance of Nanoparticles made of Manganese Dioxide using Manganese Acetate Tetrahydrate as Precursor

Anil Kumar[1], Dr. Anil Kumar Shrotriya[2]
[1]*Assistant Professor in Physics, Govt. Bangur College Didwana*
[2]*Associate Professor in Physics, S.P.S.B. Govt. College Shahpura, Rajasthan*

Abstract: ***This study describes a straightforward, effective, and environmentally benign method for producing manganese dioxide nanoparticles (MnO2 NPs) using Nyctanthes arbor-tristis leaf extract. It was discovered by Fourier-transform infrared spectra that the plant extract contributed to the creation of MnO2 NPs. The band gap of the synthesised MnO2 NPs was identified as the source of the absorption peaks observed in the UV–visible absorption spectra at 412 nm. X-ray diffraction analysis was used to identify the crystal phase of the MnO2 NPs and validate the development of crystalline MnO2 NPs. According to the X-ray diffraction pattern, MnO2 NPs have crystalline nature. Furthermore, the synthesised MnO2 NPs' was revealed by field emission scanning electron microscopy investigation with EDS which gives Information about Compositional elements. MnO2 NPs have the ability to degrade MB dyes in the UV-Visible light spectrum by photocatalysis. Using Methylene Blue as an organic pollutant, the photocatalytic activities for the dye degradation of MnO2 NPs were assessed.***
Keywords: NPs, XRD, FTIR, SEM, TEM, EDS, Biodegradable, dyedegradation, Photocatalytic activity, Green Synthesis.

I. INTRODUCTION

Nanomaterials have emerged as unique antibacterial agents with unique physicochemical features and a high surface area to volume ratio (Gatoo, Naseem, Arfat, Dar, Qasim, & Zubair, 2014). Additionally, nanomaterials are being used in medicine to find and deliver therapeutic drugs for a variety of illnesses (Bhatia, 2016). In comparison to other materials, metal nanoparticles (NPs) have superior surface area to volume ratio, surface energy, spatial confinement, and decreased imperfections. These properties make them reliable in physicochemical, electrical, mechanical, magnetic, thermal, optical, and biological processes (Joudeh & Linke, 2022). The wide range of uses for manganese oxide nanoparticles (NPs) in several sectors, including microelectronics (Xia, Wan, Yan, & Lu, 2014), chemical sensing devices (Dawadi, Gupta, Khatri, Budhathoki, Lamichhane, & parajuli, 2020), optoelectronics, rechargeable batteries, ion-sieves and catalysis (Debnath, Roy, Kapri, & Bhattacharyya, 2016), has drawn attention. Mn is the twelfth most abundant element on Earth and the third most common transition element after Fe and Ti (Hoseinpour, Souri, & Ghaemi, 2018). Moreover, because of the availability of several attachments for a variety of uses, they are based against earth additional elements. Additionally, the photocatalytic activity of manganese dioxide nanoparticles (MnO2 NPs) for dye degradation is good. The most popular methods for nanoscale synthesis include electrochemical and photochemical reduction techniques, chemical precipitation, sol-gel, solvothermal/hydrothermal, solid-state synthesis, and basic solution-based methods (Ding, Zheng, Ma, & Lin, 2020). Green fabrication is a preferable option since it is more environmentally friendly, even though physical and chemical processes can be used for nanoscale synthesis (Parveen, Banse, & Ledwani, Green Synthesis of Nanoparticles: Their Advantages and Disadvantages, 2016). Plant extracts can be used to manufacture nanoscales, which has advantages over other biological processes including the microbial method and the drawn-out process of maintaining cell cultures (jeevanandam, et al., 2022). The creation of metal and metal-oxide nanoscales is attributed to the antioxidant properties of plants. The use of extracts from numerous other herbs, including Xanthium strumarium, Euphorbia hirta, Azadirachta indica, Corriandrum sativum, Polyalthia longifolia,Camellia sinensis and Nelumbo nucifera, complies with the environmentally friendly concepts of green chemistry (Hoseinpour, Souri, & Ghaemi, 2018). This benignant reaction can be quickly and readily scaled up at room temperature and pressure. It can also be completed with ease.

As previously mentioned, utilising plant extracts for NP synthesis is referred to as a "green method." Numerous investigations, such as the synthesis of silver nanoparticles (NPs) utilising the catalytic activity of Malva parviflora leaf extract (Zayed, Eisa, & Shabaka, 2012), the synthesis of gold NPs using Phoenix dactylifera L. leaf extract (Zayed & Eisa, Phoenix dactylifera L. leaf extract phytosynthesized gold nanoparticles; controlled synthesis and catalytic activity, 2014), the biosynthesis of silver NPs using Ziziphus spina-christi, etc., all support this claim. This investigation used the green approach to generate MnO2 NPs, which were then characterised using Fourier-transform infrared (FTIR) analytical techniques, field emission scanning electron microscopy (FESEM),X-ray diffraction (XRD), ultraviolet-visible spectroscopy (UV-vis), synthesised MnO2 nanoparticles show photocatalytic activity for the breakdown of dye. The degradation of Methylene Blue dye was used to test the photocatalytic activity for dye degradation of the synthesised MnO2 NPs.

II. EXPERIMENTAL

A. Reagents

Manganese acetate tetra hydrate was bought from Fisher Scientific. methylene blue was purchased from Sigma Aldrich. DI water was taken from Organo biotech private limited. Leaves of Nyctanthes arbor-tristis plant were collected from a local garden. Whatman filter paper grade no. 1 size 125 mm was purchased from local vendor.

B. Instruments

Fourier Transform Infrared Spectroscopy (FTIR) was performed using the Shimadzu IRAffinity-1S model in Attenuated Total Reflectance (ATR) mode, covering a spectral range of 4000-400 cm^{-1}. The FTIR analysis was conducted at a resolution of 8 cm^{-1} with a scanning speed of 64 scans/min. UV-Visible (UV-Vis) Spectroscopy for analyzing nanoparticle synthesis was recorded using the Shimadzu UV 1900i model. The particle size distribution of the nanoparticles was determined via Dynamic Light Scattering (DLS) spectroscopy, employing the Litesizer 500 model from Anton Paar. The morphological patterns and elemental composition of the synthesized samples were assessed using a Field Emission Scanning Electron Microscope (FESEM), operated at an energy setting of 10 KeV (Zeiss Supra 55VP, EDAX Ametek). Prior to imaging, the samples were mounted on carbon adhesive tape affixed to an aluminum stage and sputter-coated with gold using an Emitech K550X sputter coater from Labtech International for 120 seconds. The size and morphology of the synthesized nanoparticles were further characterized using Transmission Electron Microscopy (TEM) with a Jeol Jem-1400 model. A solution containing manganese dioxide nanoparticles was deposited onto a carbon-backed copper grid, which was then dried overnight at 40°C. The crystalline nature of the synthesized nanoparticles was determined by X-Ray Diffraction (XRD) using a Rigaku Ultima IV model, scanning from 5 to 60 degrees at a rate of 2 degrees/min with a CuKα radiation source.

C. Green Synthesis and Characterisation of MnO_2 Nanoparticle using Manganese acetate tetra Hydrate as Precursor

1) Preparation of Leaf Extract

Leaf extract from Nyctanthes arbor-tristis (commonly known as night-flowering jasmine) was prepared for the synthesis of nanoparticles. Fresh leaves of N. arbor-tristis were collected, thoroughly washed with deionized water to remove any surface contaminants, and then air-dried. Subsequently, 20 grams of the clean leaves were cut into small pieces and immersed in 100 milliliters of deionized water. This mixture was heated to 60°C and maintained at this temperature for 1 hour, during which the solution gradually turned a light green color, indicating the release of phytochemicals into the aqueous medium. The resultant leaf extract was then filtered through Whatman No. 1 filter paper to remove any solid plant residues, and the filtrate was collected for subsequent nanoparticle synthesis.

2) Synthesis of MnO2 Nanoparticles

Three sets of manganese dioxide MnO2 nanoparticles were synthesized using manganese acetate tetrahydrate Mn(CH3CO2)2.4H2O as the manganese precursor. Initially, 0.1 M manganese acetate was prepared by dissolving the appropriate amount in 10 mL of deionized water. To this solution, 1 mL, 3 mL, and 6 mL of the previously prepared Nyctanthes arbor-tristis leaf extract were added dropwise under continuous magnetic stirring.

The reaction mixtures were maintained at a constant temperature of 60°C and stirred continuously for 24 hours. During this process, the color of the solution changed from colorless to light yellow, indicating the formation of MnO2 nanoparticles. The resultant nanoparticle suspensions were then collected for further characterization.

III. RESULTS AND DISCUSSIONS

A. *Fourier Transform Infrared Spectroscopy*

The formation of MnO2 nanoparticles were confirmed by FTIR in ATR mode. The leaf extract and the salt precursor were also characterized via FTIR. The Figure 1. depicted the FTIR spectra of MnO2 nanoparticles. The leaf extract spectra showed band at ~3300 cm^{-1} arising from OH stretching vibrations due to the presence of various different types of flavonoids in the leaf extract. The salt precursor also showed bands at ~3300 cm^{-1} and ~3000 cm^{-1} due to the presence of OH and methyl groups respectively. The salt precursor showed bands at ~1552 cm^{-1} and ~1400 cm^{-1} due to CO asymmetric and symmetric stretching respectively. The ~1028 cm^{-1} band in salt corresponded to CH3 bending vibrations (Pang, Wu, Zhang, & Zhang, 2015). However, two new bands at ~1163 cm^{-1} and 829 cm^{-1}appeared in the spectra of MnO2 nanoparticles. The appearance of these bands confirmed the formation of nanoparticles. However, the other peaks of salt at ~3300 cm^{-1}, ~3000 cm^{-1}, ~1552 cm^{-1}, ~1400 cm^{-1}, and ~1028 cm^{-1}got slightly shifted in the MnO2-A1, MnO2-A2, and MnO2-A3 samples due to the formation of nanoparticles.

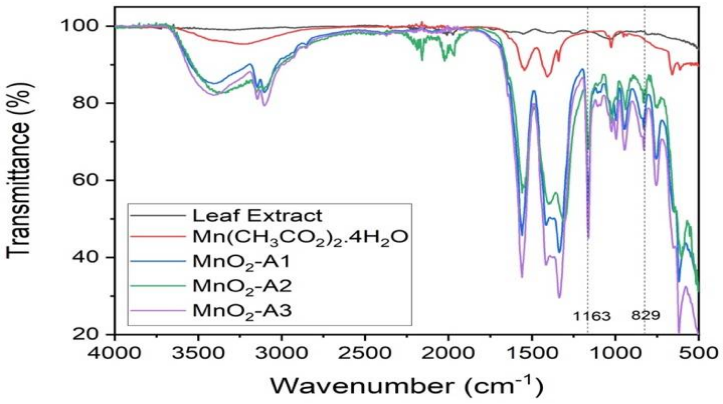

Figure 1. ATR-FTIR spectra of MnO2-A nanoparticles respectively at different concentrations of leaf extract

B. *UV-Vis Spectroscopy*

The UV-Vis absorption spectra of MnO2 nanoparticles synthesized using Mn(CH3CO2)2.4H2O exhibited a distinct peak around 412 nm(Figure 2) (Hoseinpour, Souri, & Ghaemi, Green synthesis, characterisation, and photocatalytic activity of manganese dioxide nanoparticles, 2018). This peak corresponded to the characteristic absorption band of MnO2, indicating the presence of d-d electronic transitions within the material. The absorption at this wavelength is typically associated with the charge transfer transitions between the manganese ions and oxygen ligands in the MnO2 lattice. The appearance of this peak signified the efficient light absorption capability of MnO2 nanoparticles, which was essential for their role as photocatalysts. It can also be observed from the graph that the intensity of the ~412 nm band increased with the increase in the concentration of leaf extract. The intensity of MnO2-A3 which was synthesized using 6 mL of leaf extract was the highest indicating a higher degree of transformation of precursor into nanoparticles. There was a very low intensity band in MnO2-A1 nanoparticles which utilized 1 mL of leaf extract indicating a lower degree of transformation of precursor into nanoparticles.These observations underscore the critical role of the leaf extract concentration in the synthesis process, where higher amounts of the reducing agent facilitate a more effective and complete formation of MnO2 nanoparticles.

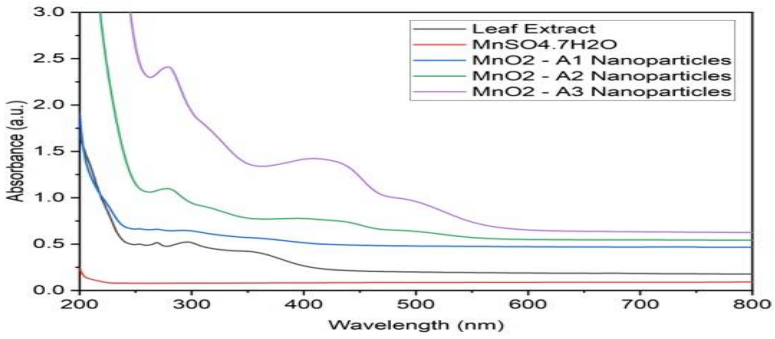

Figure 2. UV-Vis spectra of MnO2-A nanoparticles at different concentrations of leaf extract.

C. *Dynamic Light Scattering*

The size of the synthesized nanoparticles was measured using Dynamic Light Scattering (DLS), as shown in Figures 3A-3C. The results indicated that a consistent trend was observed across all nanoparticle samples, where the size decreased with an increase in the concentration of the reducing and capping agent (leaf extract). Higher concentrations of the reducing agent enhance the nucleation rate, leading to the simultaneous formation of numerous small nuclei. This dispersion of the precursor material across a large number of particles results in the formation of smaller nanoparticles. Additionally, capping agents stabilize these nanoparticles more effectively, maintaining their smaller size and uniformity. The increased concentration of these agents also slows down the growth rate by inhibiting further atomic addition to the nanoparticles, thereby ensuring controlled growth. The graphs (Figures 3A-3C) showed that the average sizes of MnO2 nanoparticles were 278 nm, 86 nm, and 47.8 nm for MnO2-A1, MnO2-A2, and MnO2-A3, respectively. The size decreased with the increase in leaf extract concentration from 1 mL to 6 mL.

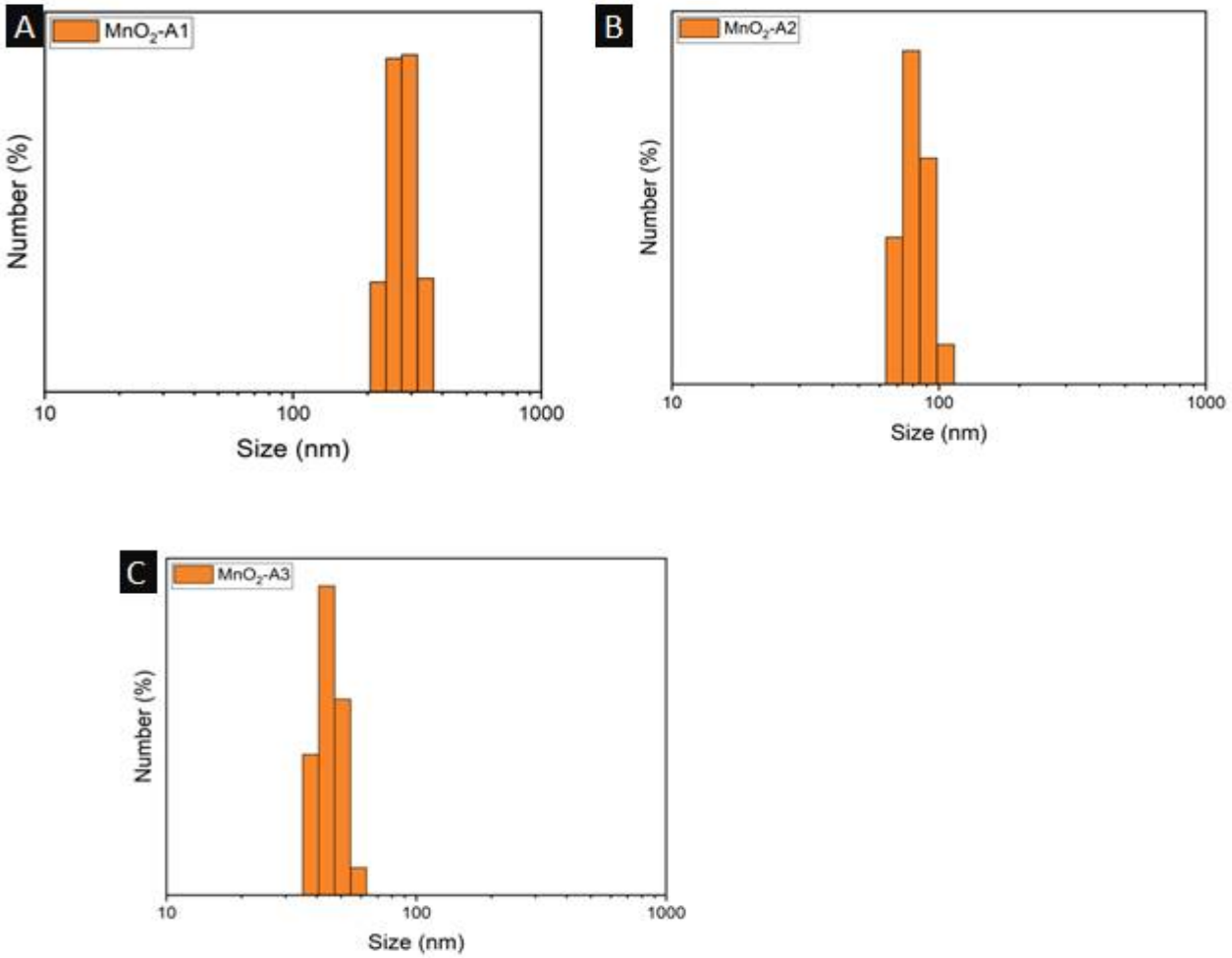

Figure 3. DLS spectra of (A) MnO2-A1, (B) MnO2-A2, (C) MnO2-A3 nanoparticles at different concentrations of leaf extract.

D. X-Ray Diffraction

The crystalline structure of MnO2 nanoparticles was analyzed using X-ray diffraction (XRD), as shown in Figure 4.The sample MnO2-A3 was chosen for further characterization and application as it showed the smallest size. The XRD pattern exhibited sharp diffraction peaks at 2θ values of 12.89°, 18.07°, 28.88°, 37.79°, 42.05°, 49.98°, 56.27°, 60.40°, and 69.77°. These peaks corresponded to the crystallographic planes (110), (200), (310), (211), (301), (411), (600), (521), and (541), respectively. The observed diffraction pattern matched well with the standard JCPDS card no. 44-0141 (Wan, et al., 2019), confirming the successful synthesis of α-MnO2 with a tetragonal crystalline structure and space group *14/m*. Additionally, the absence of peaks associated with impurities indicates that the synthesized α-MnO2 nanoparticles are of high purity. This high level of crystallinity and purity is critical for the nanoparticles' performance in various applications, as it ensures consistent and predictable behavior.

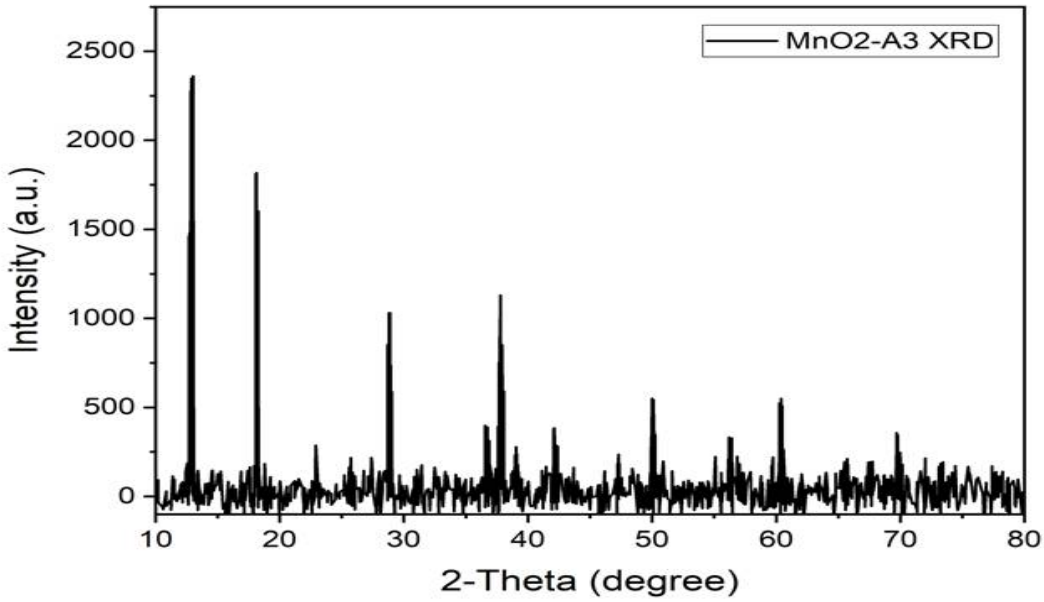

Figure 4. XRD graphs of MnO2-A3 nanoparticles.

E. Scanning Electron Microscopy and EDAX

In this analysis, nanoparticle samples MnO2-A3 was synthesized and subjected to Scanning Electron Microscopy (SEM) coupled with Energy Dispersive X-ray Spectroscopy (EDS) to ascertain their morphological and elemental composition characteristics. The SEM image of MnO2-A3 (Figure 5A) reveals its surface morphology, while the corresponding EDS elemental mapping (Figures 5B-E) and composition table (Figure 5F) indicate the presence of carbon (31.3%), oxygen (27.6%), and manganese (41.2%). These compositional analyses not only corroborate the successful synthesis of the targeted materials but also provide critical insights into their elemental distribution, essential for understanding their potential applications in various domains.

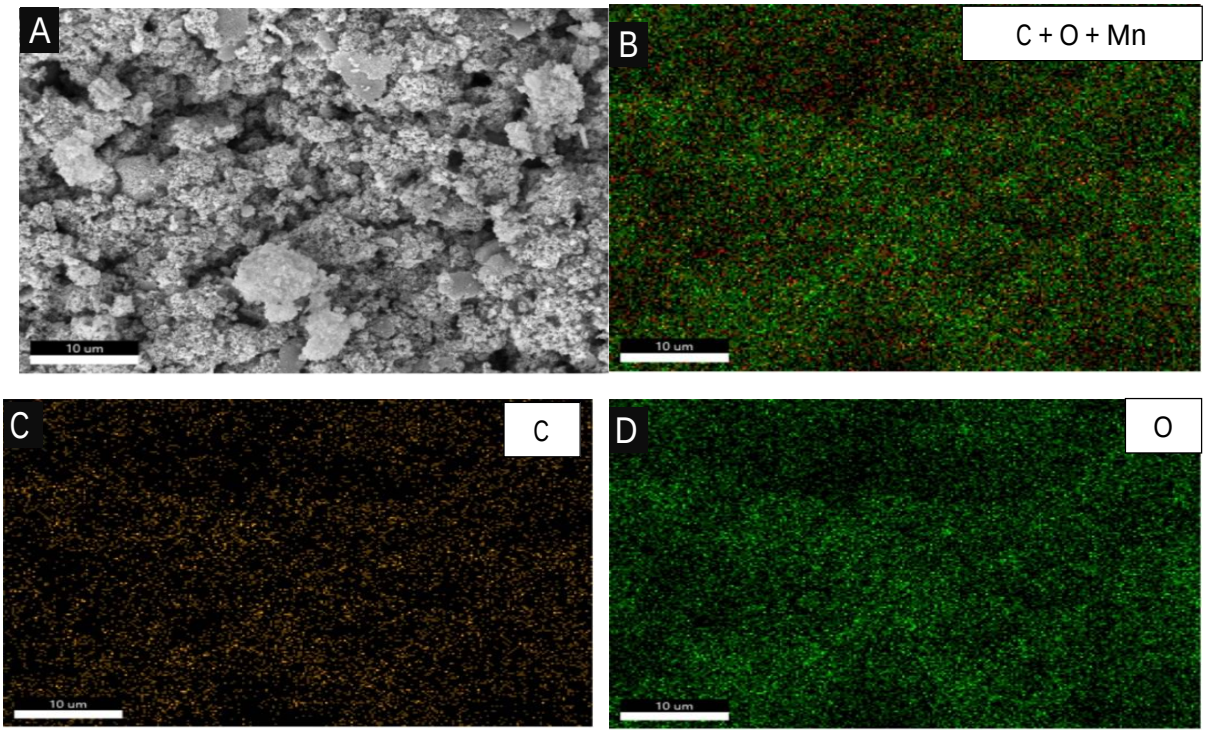

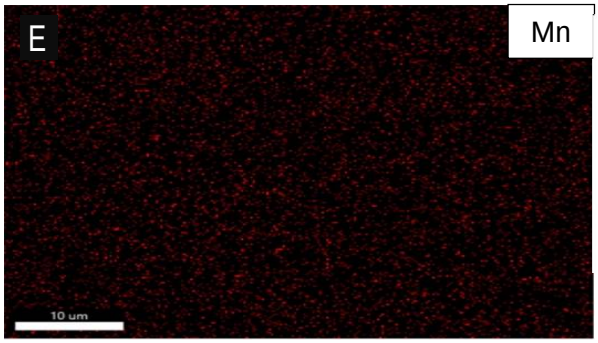

F

Element	Weight %	Atomic %	Error %
C K	31.2	51.2	9.2
O K	27.6	34.0	8.0
Mn K	41.2	14.8	7.7

Figure 5. (A)SEM image of MnO2-A3. (B) Overall elemental mapping with individual elemental mapping of (C) carbon, (D) oxygen, and (E) manganese element along with (F) composition table.

F. Transmission Electron Microscopy and Size Distribution

Figure 6 presents the Transmission Electron Microscopy (TEM) images and corresponding particle size distribution graphs for MnO2-A3nanoparticles. The TEM image of MnO2-A3 (Figure 6A) reveals its spherical morphology, with a particle size distribution centered around 50±10 nm as depicted in Figure 6B. These TEM analyses confirm the uniformity in shape and provide precise measurements of the nanoparticle sizes, critical for their application in various nanotechnological and industrial fields.

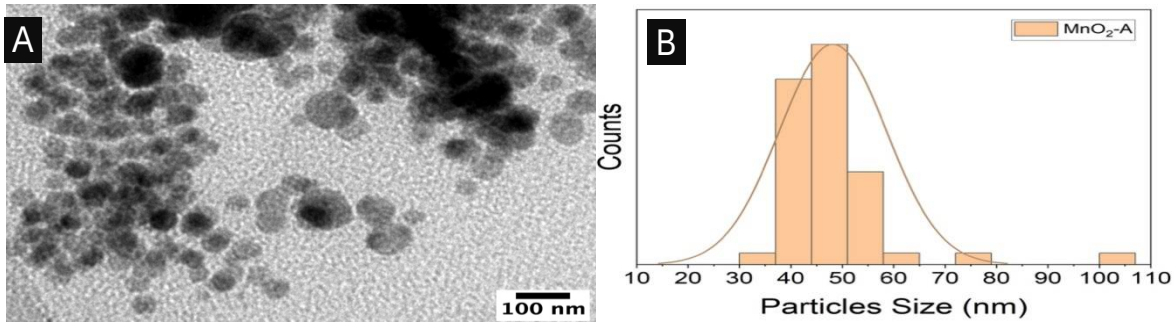

Figure 6. Showing the TEM images of (A) morphology of MnO2-A nanoparticles and its (B) particle size distribution graph.

IV. PHOTOCATALYTIC ACTIVITY OF NANOPARTICLES

A. Visual Observation and UV-Vis Study

The study aimed to investigate the degradation of Methylene Blue (MB) dye using MnO2 nanoparticles, evaluating their photocatalytic efficiency under direct sunlight over various time intervals. The photodegradation of MB dye was monitored both visually and through UV-Vis spectroscopy. Initially, the MB solution, with a starting concentration of 10 mg/L, exhibited a distinct blue colorant the zero-minute mark after the introduction of MnO2 nanoparticlesas illustrated in Figure 7. Over time, the blue coloration of the solution began to diminish, indicating the progressive breakdown of the dye. After 360 minutes of exposure to direct sunlight, the solution became nearly colorless, signifying substantial degradation of the MB dye. This observation suggests that the MnO2 nanoparticles effectively facilitated the photocatalytic degradation of the dye under solar irradiation.

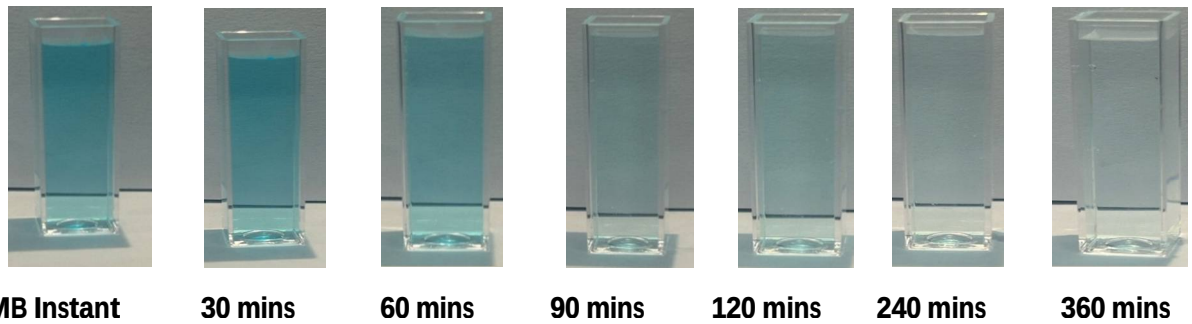

Figure 7. Visual observation of the photocatalytic degradation of MB dye by MnO2-A3 nanoparticles.

However, the photocatalytic efficiency was calculated through UV-Vis spectroscopy. The distinct absorption peak of Methylene Blue (MB) was observed at a maximum wavelength (λmax) of approximately 664 nm using a UV-Vis absorption spectrometer, a key indicator for tracking dye degradation. The initial absorbance of the MB solution was recorded prior to exposure to sunlight, with subsequent measurements taken at regular intervals to monitor changes over time. The study evaluated the effect of contact time on the photocatalytic degradation of MB dye by maintaining a constant dye concentration of 10 mg/Land a fixed nanoparticle dose of 5 mL, measuring at various intervals (0, 30, 60, 90, 120, 180, 240, and 360 minutes).Throughout the degradation process, the maximum absorption wavelength remained unchanged, while the intensity of the absorption peaks for MB progressively decreased. This trend indicated significant degradation of the dye, as shown in Figures 8A. Additionally, graphs were plotted to illustrate the degradation percentage relative to absorbance intensity over time (Figures 8B). After 360 minutes of direct sunlight exposure, the maximum photodegradation efficiencies were recorded 78.56% for MnO2-A nanoparticles. The impact of contact time was significant in the dye degradation process. Initially, up to 120 minutes, the dye degradation was relatively slow, achieving approximately 25% for MnO2-A for nanoparticles. However, as the contact time increased, the degradation rate accelerated, reaching maximum degradation levels after 360 minutes. This enhanced degradation over extended contact times underscores the importance of sustained exposure for effective photocatalytic activity.

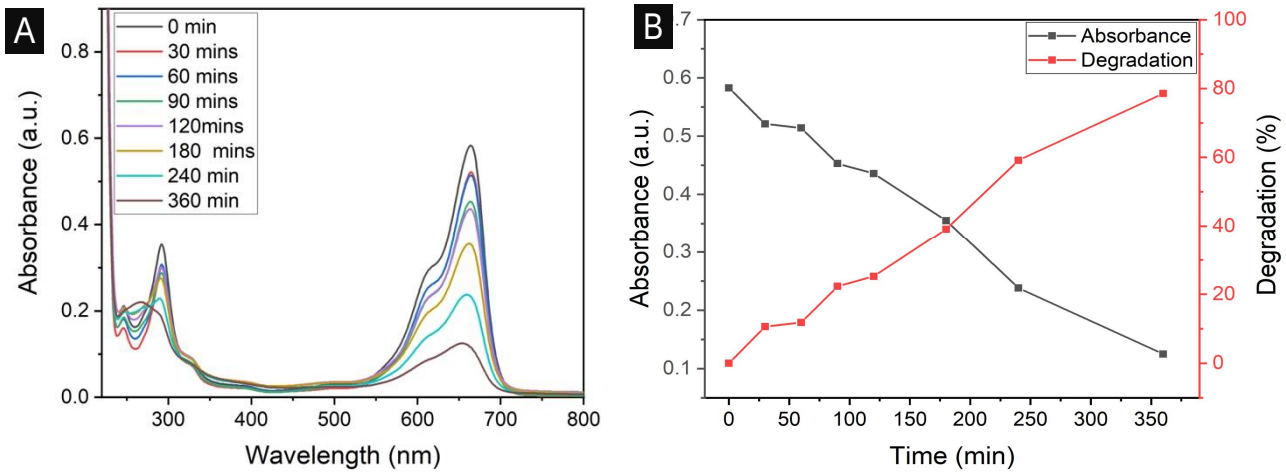

Figure 8. The graphs of photodegradation of methylene blue dye (A) Absorbance spectra, (B) Effect of time on degradation percentage by MnO2-A3 nanoparticles

V. KINETIC STUDY OF DYE DEGRADATION

The degradation of Methylene Blue (MB) using the synthesized nanoparticles adhered to a kinetic model known as pseudo-first-order kinetics, which is based on a modified Langmuir-Hinshelwood approach (kumar, thakur, kumar, & jeet, 2023) (Abu-Dief, Essawy, diab, & mohamed, 2021) (Hashemi, Poursalehi, & Delavari, 2022).

$$ln\ \frac{C}{C_0} = -kt$$

where, Co and C are the initial and final concentration of Mb dye in the solution, k is the rate constant, and t is the contact time.
The above equation can be adapted accordingly (Goudjil, Dali, Zighmi, Mahcene, & Bencheikh, 2024) as shown below:

$$ln\ \frac{A}{A_0} = -kt$$

In this context, the initial concentration of the dye is denoted as C_0, with its corresponding absorbance value represented as A_0. Following irradiation, the dye concentration is represented as C, and the corresponding absorbance value is denoted as A. The data was plotted for ln (A/A_0) versus time, as shown in Figure 9A. Applying the first-order kinetics principle yielded a good linear fit, with regression coefficients of 0.974 for MnO2-A nanoparticles, as depicted in Figures 9B. The calculated rate constants for the photodegradation process were found to be 0.00495 per minute for MnO2-A nanoparticles. These rate constants further confirmed that MnO2-A nanoparticles exhibit the highest efficiency for MB dye degradation.This enhanced efficiency of MnO2-A nanoparticles can be attributed to the synthesis method using Mn(CH3CO2)2.4H2O as the precursor, which resulted in smallest sized nanoparticles.

The reduced size of these nanoparticles increased the surface area available for adsorption sites when exposed to direct sunlight, facilitating the production of free radicals. These free radicals have a higher likelihood of interacting with MB dye molecules, thereby contributing to the observed maximum degradation (kalaycioglu, uysal, pekcan, & erim, 2023)

In summary, the pseudo-first-order kinetics model provided a reliable framework for understanding the photodegradation of MB dye by MnO2 nanoparticles. The differences in rate constants and degradation efficiencies highlighted the critical role of nanoparticle size and surface area in enhancing photocatalytic activity under sunlight.

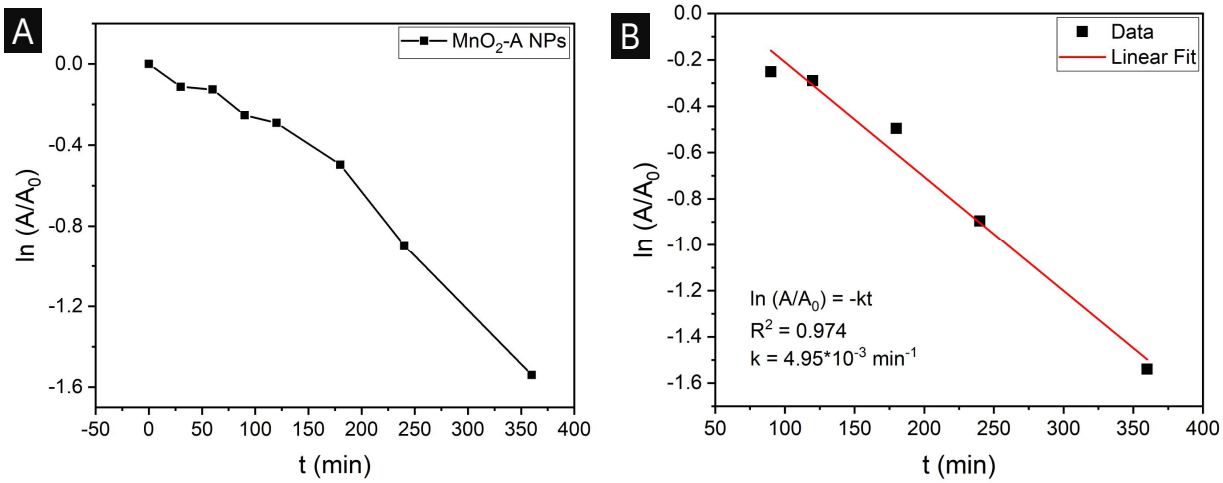

Figure 9 (A) Kinetic measurement of MB dye photodegradation, (B) Linear fitting model of kinetic measurement by MnO2-A3 nanoparticles.

VI. CONCLUSIONS

The synthesis and characterization of MnO2 nanoparticles using Nyctanthesarbor-tristis leaf extract have demonstrated the potential for green chemistry approaches in nanomaterial production. The comprehensive analysis of the synthesized nanoparticles revealed significant insights into their structural, morphological, and functional properties. The UV-Vis spectroscopy results demonstrated the efficient formation of MnO2 nanoparticles, with distinct absorption peaks at 412 nm, indicating their potential photocatalytic properties. The Dynamic Light Scattering (DLS) analysis confirmed that the size of the nanoparticles decreased with an increase in the concentration of the leaf extract, emphasizing the crucial role of the reducing and capping agent in controlling nanoparticle dimensions. X-ray diffraction (XRD) patterns confirmed the crystalline structures of MnO2 nanoparticles, demonstrating high purity and crystallinity, which are essential for their performance in various applications. Fourier Transform Infrared Spectroscopy (FTIR) further validated the formation of nanoparticles, with the appearance of new bands and shifts in existing bands indicating successful synthesis. Scanning Electron Microscopy (SEM) coupled with Energy Dispersive X-ray Spectroscopy (EDS) provided detailed morphological and elemental composition analysis, confirming the presence of key elements and supporting the successful synthesis of the targeted nanoparticles. Transmission Electron Microscopy (TEM) images and particle size distribution analyses revealed uniformity in shape and precise measurements of nanoparticle sizes, essential for their application in nanotechnology and industry. The synthesis process employed in this study offered significant advantages over conventional methods, primarily due to its eco-friendliness and sustainability. By utilizing Nyctanthesarbor-tristis leaf extract as a reducing and capping agent, the need for hazardous chemicals was eliminated, making the process safer and more environmentally benign. This approach aligned with the principles of green chemistry, promoting the use of renewable resources and reducing waste generation.

The photocatalytic efficiency of the nanoparticles was evaluated through the degradation of Methylene Blue (MB) dye under direct sunlight. The UV-Vis spectroscopy data showed a significant decrease in the intensity of the characteristic absorption peak of MB, indicating substantial degradation of the dye. The study revealed that the photocatalytic efficiency with MnO2 (synthesized using Mn(CH3CO2)2.4H2O) achieving a 78.56% degradation rate after 360 minutes of sunlight exposure. The kinetic study of dye degradation followed pseudo-first-order kinetics, with calculated rate constants further confirming the superior photocatalytic activity of the composite. The comprehensive analysis underscored the influence of synthesis conditions, particularly the concentration of the leaf extract, on the structural and functional properties of the nanoparticles. The findings highlighted the potential of these biogenically synthesized MnO2 nanoparticles for efficient photocatalytic applications, emphasizing the critical role of nanoparticle size, surface area, and purity in enhancing their performance.

REFERENCES

[1] Abu-Dief, A. M., Essawy, A. A., Diab, A. K., & Mohamed, W. S. (2021). Facile synthesis and characterization of novel Gd2O3–CdO binary mixed oxide nanocomposites of highly photocatalytic activity for wastewater remediation under solar illumination. Journal of Physics and Chemistry of Solids, 148, 109666.
[2] Bhatia, S., & Bhatia, S. (2016). Nanoparticles types, classification, characterization, fabrication methods and drug delivery applications. Natural polymer drug delivery systems: Nanoparticles, plants, and algae, 33-93.
[3] Dawadi, S., Gupta, A., Khatri, M., Budhathoki, B., Lamichhane, G., & Parajuli, N. (2020). Manganese dioxide nanoparticles: synthesis, application and challenges. Bulletin of Materials Science, 43, 1-10.
[4] Debnath, B., Roy, A. S., Kapri, S., & Bhattacharyya, S. (2016). Efficient dye degradation catalyzed by manganese oxide nanoparticles and the role of cation valence. ChemistrySelect, 1(14), 4265-4273.
[5] Ding, B., Zheng, P., Ma, P. A., & Lin, J. (2020). Manganese oxide nanomaterials: synthesis, properties, and theranostic applications. Advanced Materials, 32(10), 1905823.
[6] Gatoo, M. A., Naseem, S., Arfat, M. Y., Mahmood Dar, A., Qasim, K., & Zubair, S. (2014). Physicochemical properties of nanomaterials: implication in associated toxic manifestations. BioMed research international, 2014(1), 498420.
[7] Goudjil, M. B., Dali, H., Zighmi, S., Mahcene, Z., & Bencheikh, S. E. (2024). Photocatalytic degradation of methylene blue dye with biosynthesized Hematite α-Fe2O3 nanoparticles under UV-Irradiation. Desalination and Water Treatment, 317, 100079.
[8] Hashemi, E., Poursalehi, R., & Delavari, H. (2022). Structural, optical and photocatalytic activity of multi-heterojunction Bi2O3/Bi2O2CO3/(BiO) 4CO3 (OH) 2 nanoflakes synthesized via submerged DC electrical discharge in urea solution. Nanoscale Research Letters, 17(1), 75.
[9] Hoseinpour, V., Souri, M., & Ghaemi, N. (2018). Green synthesis, characterisation, and photocatalytic activity of manganese dioxide nanoparticles. Micro & Nano Letters, 13(11), 1560-1563.
[10] Jeevanandam, J., Kiew, S. F., Boakye-Ansah, S., Lau, S. Y., Barhoum, A., Danquah, M. K., & Rodrigues, J. (2022). Green approaches for the synthesis of metal and metal oxide nanoparticles using microbial and plant extracts. Nanoscale, 14(7), 2534-2571.
[11] Joudeh, N., & Linke, D. (2022). Nanoparticle classification, physicochemical properties, characterization, and applications: a comprehensive review for biologists. Journal of Nanobiotechnology, 20(1), 262.
[12] Kalaycıoğlu, Z., Özuğur Uysal, B., Pekcan, O., & Erim, F. B. (2023). Efficient photocatalytic degradation of methylene blue dye from aqueous solution with cerium oxide nanoparticles and graphene oxide-doped polyacrylamide. ACS omega, 8(14), 13004-13015.
[13] Pang, S. F., Wu, C. Q., Zhang, Q. N., & Zhang, Y. H. (2015). The structural evolution of magnesium acetate complex in aerosols by FTIR–ATR spectra. Journal of Molecular Structure, 1087, 46-50.
[14] Parveen, K., Banse, V., & Ledwani, L. (2016, April). Green synthesis of nanoparticles: Their advantages and disadvantages. In AIP conference proceedings (Vol. 1724, No. 1). AIP Publishing.
[15] Wan, X., Yang, S., Cai, Z., He, Q., Ye, Y., Xia, Y., ... & Liu, J. (2019). Facile synthesis of MnO2 nanoflowers/N-doped reduced graphene oxide composite and its application for simultaneous determination of dopamine and uric acid. Nanomaterials, 9(6), 847.
[16] Xia, H., Wan, Y., Yan, F., & Lu, L. (2014). Manganese oxide thin films prepared by pulsed laser deposition for thin film microbatteries. Materials Chemistry and Physics, 143(2), 720-727.
[17] Zayed, M. F., & Eisa, W. H. (2014). Phoenix dactylifera L. leaf extract phytosynthesized gold nanoparticles; controlled synthesis and catalytic activity. Spectrochimica Acta Part A: Molecular and Biomolecular Spectroscopy, 121, 238-244.
[18] Zayed, M. F., Eisa, W. H., & Shabaka, A. A. (2012). Malva parviflora extract assisted green synthesis of silver nanoparticles. Spectrochimica Acta Part A: Molecular and Biomolecular Spectroscopy, 98, 423-428.

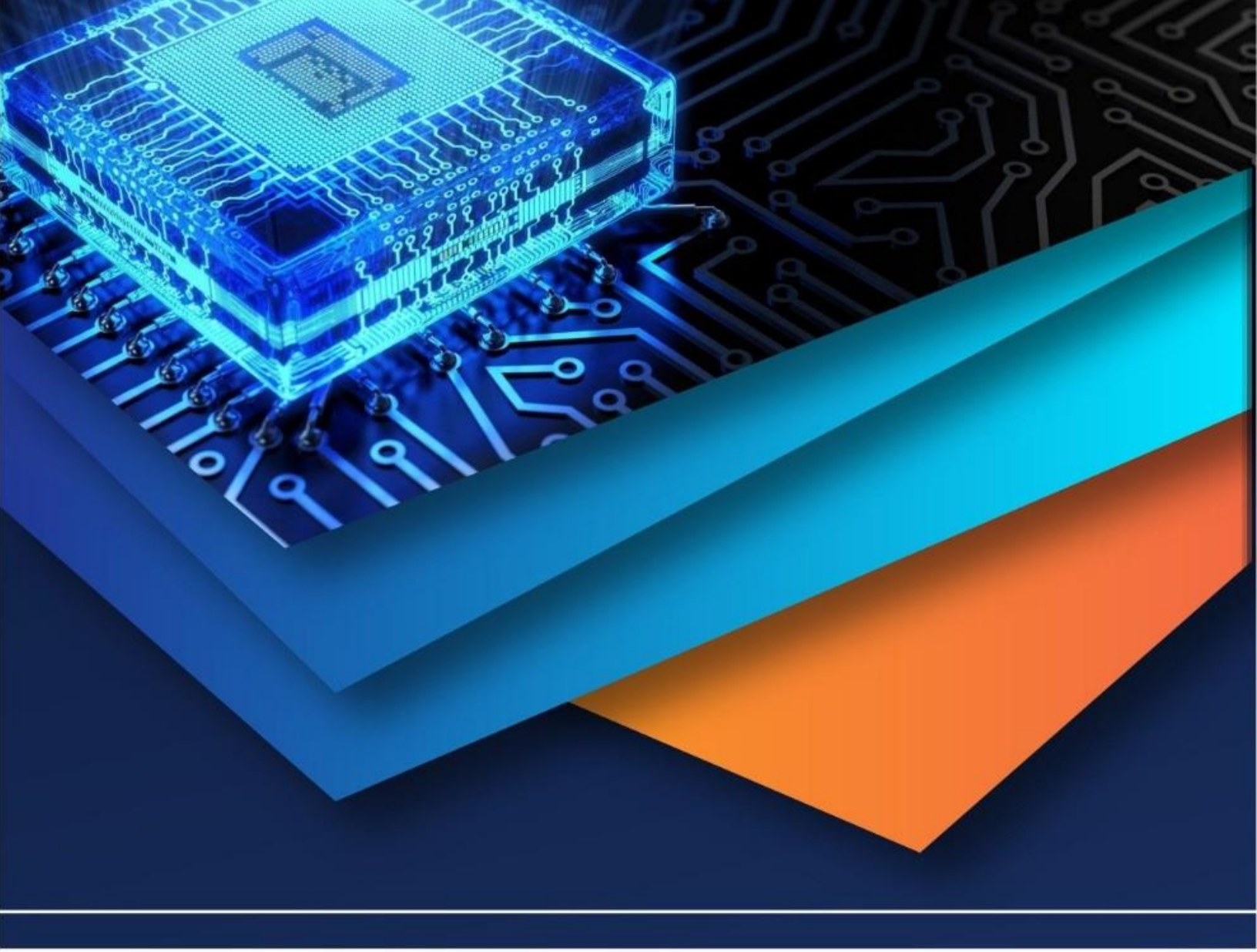

10.22214/IJRASET

45.98

IMPACT FACTOR: 7.129

IMPACT FACTOR: 7.429

INTERNATIONAL JOURNAL FOR RESEARCH

IN APPLIED SCIENCE & ENGINEERING TECHNOLOGY